The Journal of Child Psychology and Psychiatry

Journal of Child Psychology and Psychiatry **:* (2022), pp **–** doi:10.1111/jcpp.13749

Adolescent functional network connectivity prospectively predicts adult anxiety symptoms related to perceived COVID-19 economic adversity

Felicia A. Hardi,[1] Leigh G. Goetschius,[2] Vonnie McLoyd,[1] Nestor L. Lopez-Duran,[1] Colter Mitchell,[3,4] Luke W. Hyde,[1,3] Adriene M. Beltz,[1] and Christopher S. Monk[1,3,5,6]

[1]Department of Psychology, University of Michigan, Ann Arbor, MI, USA; [2]The Hilltop Institute, University of Maryland Baltimore County, Baltimore, MD, USA; [3]Survey Research Center of the Institute for Social Research, University of Michigan, Ann Arbor, MI, USA; [4]Population Studies Center of the Institute for Social Research, University of Michigan, Ann Arbor, MI, USA; [5]Neuroscience Graduate Program University of Michigan, Ann Arbor, MI, USA; [6]Department of Psychiatry, University of Michigan, Ann Arbor, MI, USA

Background: Stressful events, such as the COVID-19 pandemic, are major contributors to anxiety and depression, but only a subset of individuals develop psychopathology. In a population-based sample (N = 174) with a high representation of marginalized individuals, this study examined adolescent functional network connectivity as a marker of susceptibility to anxiety and depression in the context of adverse experiences. **Methods:** Data-driven network-based subgroups were identified using an unsupervised community detection algorithm within functional neural connectivity. Neuroimaging data collected during emotion processing (age 15) were extracted from a priori regions of interest linked to anxiety and depression. Symptoms were self-reported at ages 15, 17, and 21 (during COVID-19). During COVID-19, participants reported on pandemic-related economic adversity. Differences across subgroup networks were first examined, then subgroup membership and subgroup–adversity interaction were tested to predict change in symptoms over time. **Results:** Two subgroups were identified: Subgroup A, characterized by relatively greater neural network variation (i.e., heterogeneity) and density with more connections involving the amygdala, subgenual cingulate, and ventral striatum; and the more homogenous Subgroup B, with more connections involving the insula and dorsal anterior cingulate. Accounting for initial symptoms, subgroup A individuals had greater increases in symptoms across time (β = .138, p = .042), and this result remained after adjusting for additional covariates (β = .194, p = .023). Furthermore, there was a subgroup–adversity interaction: compared with Subgroup B, Subgroup A reported greater anxiety during the pandemic in response to reported economic adversity (β = .307, p = .006), and this remained after accounting for initial symptoms and many covariates (β = .237, p = .021). **Conclusions:** A subgrouping algorithm identified young adults who were susceptible to adversity using their personalized functional network profiles derived from a priori brain regions. These results highlight potential prospective neural signatures involving heterogeneous emotion networks that predict individuals at the greatest risk for anxiety when experiencing adverse events. **Keywords:** Stress susceptibility; anxiety; functional connectivity; person-specific network.

Introduction

The COVID-19 pandemic is an unprecedented crisis that has increased the prevalence of mental disorders through profound stressors, including financial hardship, health concerns, and social isolation (Xiong et al., 2020), especially for marginalized and underserved communities that are disproportionately impacted due to systemic inequities (Tai, Shah, Doubeni, Sia, & Wieland, 2021). Although highly stressful experiences often precipitate anxiety and depression (McLaughlin & Nolen-Hoeksema, 2012), only a subset of individuals develops these disorders, potentially due to an increased biological sensitivity to environmental context (Boyce & Ellis, 2005). Young adults may be particularly vulnerable to the stressful impact of the pandemic, given that adolescence and young adulthood are critical developmental stages for neural change as well as shifts in social, occupational, and economic contexts. Further, approximately half of mental health symptoms begin during adolescence and about three quarters manifest before age 24 (Kessler et al., 2005), suggesting that stress susceptibility during these periods may be key in forecasting future anxiety and depression.

Studies have attempted to identify neural signatures from individuals who are more susceptible to stress, finding modest predictive links between brain function during active emotion processing with later anxiety and depression (Mattson, Hyde, Shaw, Forbes, & Monk, 2016; Swartz, Knodt, Radtke, & Hariri, 2015). Many studies linking brain function to psychopathology have utilized univariate contrast-based methods that average data across time and individuals (Elliott et al., 2020; Gordon et al., 2017), and recent methodological advances show that multivariate network-based approaches may yield more reliable and predictive estimates of

Conflict of interest statement: The authors declare that they have no conflict of interest.

dynamic neural activity (Kragel, Han, Kraynak, Gianaros, & Wager, 2021; Noble, Scheinost, & Constable, 2021; Taxali, Angstadt, Rutherford, & Sripada, 2021). Additionally, much of the literature focusing on the neural network has utilized neuroimaging data collected at rest; however, without the presence of tasks, resting scans may introduce heterogeneity in cognitive processes that individuals are engaging in during the scan (e.g., one participant may be close to sleep, whereas another is making lists), leading to greater variance in neural function (Finn, 2021). In contrast, neuroimaging during behavioral tasks may impose boundaries for the neural activity that could facilitate better prediction of clinically relevant traits (Finn et al., 2017; Greene, Gao, Scheinost, & Constable, 2018).

In the present investigation, we employed a within-person (in this case, person-specific) approach to map functional connectivity during an emotion task among select neural regions to cluster individuals with similar patterns of connectivity using a data-driven algorithm. This method grouped individuals into subgroups based on similarities and differences in their person-specific networks, thus identifying patterns of heterogeneity (i.e., greater variations in their person-specific connectivity) and homogeneity (i.e., fewer variations in connectivity). Combining hypothesis-driven model-based approaches and data-driven algorithms provides a powerful way to identify patterns of connectivity or clusters of individuals without a priori clustering assumptions; this maximizes power by leveraging the within-person nature of functional time series as well as the between-person sample size. We focused on the frontostriatal-limbic circuitry (i.e., amygdala, striatum, insula, cingulate, prefrontal cortex) that is implicated in anxiety- and depression-like behaviors in both animal models and clinical samples (Etkin & Wager, 2007; Janiri et al., 2020; Price & Drevets, 2010). In addition to clustering individuals based on their functional network, connectivity was characterized in several ways, including network density (i.e., connections within a network) and centrality (i.e., connections involving specific regions of a network; Bullmore & Sporns, 2009), revealing both comprehensive brain patterns as well as distinct roles of specific brain regions within networks.

Critically, beyond identifying specific neural patterns that could predict future anxiety and depression, there is a need to examine the psychological impact of stress within groups of individuals who are underrepresented in neuroimaging research and are at increased risk for stress exposure (Falk et al., 2013). The present study examined neural networks relating to stress susceptibility in a sample of 174 young adults with a substantial representation of African Americans and low-income families, and tested the following hypotheses: (a) that data-driven neural connectivity network would identify subgroups of adolescents with new onset or worsening symptoms of anxiety and depression 6 years later during a highly stressful period (COVID-19 pandemic); and (b) these adolescent functional network subgroupings would show differential anxiety and depression susceptibility to COVID-19 adversity. These questions were examined using functional network analyses at a critical time for neural development (age 15) to predict an escalation in symptoms over time as well as in response to adversity. Moreover, given the divergent rates of anxiety and depression among men and women (Kessler et al., 1994), and the potential effect of demographical differences and early experiences, we examined sex differences in these associations.

Methods

Sample and procedures

Participants were recruited from the Fragile Families and Child Wellbeing Study (FFCWS), a population-based sample of 4,898 children born in large US cities (population over 200,000) with an oversampling (3:1) for non-marital births, which resulted in a high representation of low-income families (Reichman, Teitler, Garfinkel, & McLanahan, 2001). When children were 15–17 years old, a cohort of 237 families from midwestern cities (Detroit, MI; Toledo, OH; Chicago, IL) was invited to participate in the Study of Adolescent Neural Development at the University of Michigan, Ann Arbor, where all neuroimaging data and symptom indicators included in this study were collected. Of these 237 youths who participated in the study, magnetic resonance imaging (MRI) data from 174 youths (mean age 15.9 years) were collected (see Appendix S1 and Figure S1 for exclusion criteria). At baseline, the included sample was 54% female and 76% African American, with a median household income of $37,000. Two years after their first visit, youth were recontacted and 128 participants were assessed over the phone. Six years after their first visit (during the pandemic), 119 participants completed online/phone assessments. These data were collected during the peak of the early waves of the pandemic (the first participant data were collected on April 30, 2020; the last participant data were collected on June 26, 2021). Participants did not differ in demographic characteristics across each wave or the full sample (Table S1). Study participants provided informed consent or assent (when minors, with parent consent) at all timepoints. Study protocols were approved by the University of Michigan ethics committee (IRB: HUM00167754; HUM00074392).

Neuroimaging measures

Functional MRI (fMRI) acquisition, task paradigm, and processing. Magnetic resonance imagings were acquired using a 3T GE Discovery MR750 scanner with an eight-channel head coil. Participants completed an emotion faces task in which they identified the gender of the actor (counterbalanced for gender and race). Functional data of each participant across all emotion trials (fear, happy, sad, neutral, and angry) during the entire task (including cross-hairs presentation) were extracted for subsequent processing (see Figure S2 for task paradigm). This approach was taken to maximize power and avoid confounds associated with contrast modeling. Standard fMRI preprocessing pipelines were utilized using detailed codes in FSL v6.0 (Beltz, Dotterer, & Goetschius, 2019; details on MRI data acquisition, task paradigm, and preprocessing are available in Appendices S2

and S3). After preprocessing, time-series functional data were extracted from seven bilateral regions of interest (ROIs): amygdala, dorsal anterior cingulate, dorsomedial prefrontal cortex, insula, orbitofrontal cortex, subgenual anterior cingulate, and ventral striatum. ROIs were 8 mm-diameter spheres centered around corresponding Montreal Neurological Institute (MNI) coordinates (Table S2) extracted from NeuroSynth (Yarkoni, Poldrack, Nichols, Van Essen, & Wager, 2011), a meta-analytic tool for establishing neural peak activation, and preregistered prior to analyses (see Appendix S4 for additional information on ROI selection and data extraction). To ensure that results pertained to the functional network connectivity of hypothesized ROIs, a sensitivity analysis was completed in which functional connectivity was estimated from other ROIs as a comparison network that was not hypothesized to predict susceptibility to stress (e.g., areas of the brain pertaining to audio, visual, sensorimotor, language processing), and the resulting subgroup memberships were compared (see Appendix S5 for details of comparison network, Table S3 for MNI coordinates of comparison ROIs, and Table S4 for comparison of resulting subgroups).

Anxiety and depressive symptoms

Symptoms were based on self-reported measures. Anxiety symptoms were measured using Screen for Child Anxiety-Related Disorders at wave 1 (baseline) and wave 2 (pre-COVID) and using the Beck Anxiety Inventory at wave 3 (COVID-19). Depressive symptoms were measured using the Mood and Feelings Questionnaire in waves 1 and 2 and using Beck Depression Inventory at wave 3. Scales showed good internal reliability across all waves (see Appendix S6). Initial (wave 1) anxiety symptoms were related to symptoms at both wave 2 (r = .58, p < .001) and wave 3 (r = .31, p < .001); anxiety at waves 2 and 3 were related at r = .58, p < .001. Initial depression symptoms were related to depression at wave 2 (r = .39, p < .001) and wave 3 (r = .38, p < .001), and symptoms at waves 2 and 3 were related at r = .42, p < .001. Standardized scores were utilized in subsequent analyses.

COVID-19 economic adversity

At wave 3, participants self-reported economic adversity experienced relating to the pandemic (M = 2.08, SD = 1.71). Participants reported yes (1) or no (0) on employment loss due to the COVID-19 pandemic and income loss due to the COVID-19 pandemic. Participants also reported on the financial state of their household: comfortable (0), enough but not extra (1), have to cut back (2), or cannot make ends meet (3); and any food scarcity experienced by the household: no food insecurity (0), sometimes (1), and often (2). These questions were scaled and then summed to compute the economic adversity score (Cronbach's α = .72), with higher scores denoting greater pandemic economic adversity. Mean-centered scores were utilized in interaction models to aid interpretation and reduce collinearity (Robinson, & Schumacker, 2009).

Covariates

To account for confounding effects, the following covariates were added to statistical models in sensitivity analyses: sex (parent-report: male, female), age during fMRI scan (in years), pubertal development (youth-report), ethnoracial identity (youth-report: Black, white, Hispanic, other/multiracial; a social construct included to account for the impacts of unmeasured structural racism), annual household income at baseline (age 15; parent-report), pandemic duration (number of days since the study commenced, April 20, 2020; to account for differences in the timing of participation), framewise displacement, early adversity (parent-report: violence exposure); social deprivation (Hein et al., 2020), cognitive ability (reading comprehension); mathematical abilities (Woodcock, McGrew, & Mather, 2001), cohabitation status (self-report: living with a partner or not), parental status (self-report: living with a child or not). See Appendix S7 for details of each covariate.

Statistical analyses

Data-driven analysis: Subgrouping group iterative multiple model estimation (S-GIMME). Statistical analyses were conducted in R, v4.0.3. S-GIMME (Gates, Lane, Varangis, Giovanello, & Guiskewicz, 2017) was applied to extracted functional time-series data. S-GIMME iteratively estimates person-specific unified structural equation models, which contain both positive and negative directed first-order lagged and contemporaneous connections among a priori ROIs; those connections can apply to everyone in a sample (reflecting homogeneity), a subset of individuals in a sample (when a subgrouping algorithm is applied through S-GIMME), or just an individual (reflecting heterogeneity). Default GIMME parameters established and supported by large-scale simulation studies (Gates et al., 2017; Gates & Molenaar, 2012; Lane, Gates, Pike, Beltz, & Wright, 2019) were used in the present investigation. Beginning with a null model, group-level connections were added for everyone if they significantly improved model fit for at least 75% of the sample as determined by the Lagrange Multiplier tests (Lütkepohl, 2005), then individuals were classified into subgroups using a Walktrap unsupervised community detection algorithm (Gates et al., 2017), which clusters individuals into data-driven subgroups without any a priori clustering assumptions and without averaging data across individuals. Finally, subgroup-level connections were added for everyone in a subgroup if they significantly improved model fit for at least 50% of members as determined by Lagrange Multiplier tests. Individual-level connections were estimated for each person (again based on the Lagrange Multiplier test) until the networks fit well, and contemporaneous edges were then extracted for subsequent analyses, consistent with previous investigations (e.g., Goetschius et al., 2020). See Appendix S8 for more information and Figure S3 for a visual representation of the S-GIMME process. GIMME and S-GIMME are validated and reliable person-specific functional connectivity analysis approaches that have been used or discussed in over 300 scientific articles (Beltz & Gates, 2017). GIMME outperformed 38 commonly-used approaches in modeling functional connectivity (Gates & Molenaar, 2012), and S-GIMME has high precision and recall in estimating connections in large-scale simulations of data with similar properties (length and sample size) as this study (Lane et al., 2019). In this study, several robustness checks were performed: psi values were examined to ensure model overfit did not affect inferences; split-half reliability was examined by applying S-GIMME separately to odd versus even volumes of the functional data to ensure data reliability; lastly, S-GIMME was applied to five randomly drawn subsamples, containing 80% of participants (Figure S4), to ensure stability in subgroup estimation. More details on each procedure are available in Appendix S9.

Subgroup differences analyses. Demographic characteristics in resulting S-GIMME subgroups were first examined using Welsch t tests to account for the heterogeneity of variances between groups. Then, subgroup network characteristics (i.e., density, node centrality) were compared between groups. Density was computed as the number of actual contemporaneous connections divided by the total number of possible connections (Bassett & Bullmore, 2017). Node

centrality was computed as a proportion of contemporaneous connections attached to corresponding nodes (i.e., ROIs) from the number of overall contemporaneous connections. Next, two linear multilevel growth curves were estimated separately for anxiety and depression to examine changes in anxiety and depression across three waves. Waves were nested within participants using unstructured error covariance matrices for random intercepts and slopes. Individual intercepts and slopes were then extracted from each model for subsequent analyses. Next, to isolate subgroup differences in symptom change over time, functional network-derived subgroup memberships and intercept (individual symptoms at wave 1; age 15) were used to predict slope (change over waves across ages 15, 17, and 21). As sensitivity analyses, covariates were added in sequential order: main covariates (i.e., age, pubertal development, gender, ethnoracial identity, income, study days), followed by additional sensitivity covariates (i.e., motion, violence exposure, social deprivation, reading comprehension, mathematical abilities, residential status with partners and/or children during the pandemic; see Appendix S10 for robustness checks). A similar approach was taken to probe ROI specificity by examining the associations between each region node centrality predicting change in anxiety and depressive symptoms over time while adjusting for the initial level of symptoms. To account for multiple comparisons, models including node centrality were Bonferroni-corrected (noted by $p_{\text{-adjust}}$). Finally, to probe sex differences, associations between sex and symptoms were examined at each timepoint, and subgroup–sex interactions were tested to predict symptoms.

Subgroup–adversity interaction analyses. The main effects between reported COVID-19 economic adversity with symptoms at wave 3 (during the pandemic) were first tested for anxiety and depression separately. Then, interactions between subgroup–adversity and symptoms (at wave 3; during the pandemic) were tested to examine whether there were subgroup differences in COVID-19 stress susceptibility. In subsequent steps, models were examined with the inclusion of initial symptoms (i.e., individual intercepts from growth curves), main covariates, and additional covariates as sensitivity analyses.

Results

Adolescent data-driven neural network subgroups

S-GIMME derived a two-subgroup model with excellent fit (average model fit indices: root mean square error of approximation = .051, standard root mean residual = .050, nonnormed fit index = .924, confirmatory fit index = .952). Subgroup B (N = 94) individuals were older and more advanced in pubertal development than Subgroup A (N = 80) individuals, but there were no significant differences in other demographic characteristics across the two subgroups (Table 1). There were significant subgroup differences in network characteristics. First,

Table 1 Characteristics of neural-based subgroups (N = 174)

	Subgroup A (N = 80)		Subgroup B (N = 94)		Statistical comparison	
Measure	Mean	*SD*	Mean	*SD*	*t*	*p*
Age during fMRI scan (years)	15.78	.51	15.94	.53	−2.02	.045
Pubertal development	3.15	.59	3.35	.55	−2.29	.024
Anxiety (wave 1)[1]	17.27	11.33	17.14	11.17	.07	.941
Anxiety (wave 2)[1]	16.51	12.34	14.93	12.22	.72	.475
Anxiety (wave 3; COVID-19)[1]	12.62	13.01	8.67	10.34	1.80	.074
Depression (wave 1)[2]	15.52	10.08	15.43	9.96	.06	.951
Depression (wave 2)[2]	15.37	14.25	12.36	12.44	1.24	.220
Depression (wave 3; COVID-19)[2]	11.91	8.69	10.32	8.53	1.00	.320
COVID-19 economic adversity	2.22	1.67	1.97	1.74	.78	.439
Days since study commenced	168.90	99.10	140.66	84.28	1.75	.083
	N	%	*N*	%	χ^2	*p*
Sex						
Female	43	53.75	51	54.26	0	1
Male	37	46.25	43	45.74		
Ethnoracial identity[3]						
Black	63	78.75	70	74.47	0.47	.789
White	9	11.25	12	12.77		
Hispanic/LatinX	5	6.25	7	7.45		
Other/Multiracial	3	3.75	5	5.32		
Annual household income (baseline at wave 1)[4]						
<$15,000	24	30	17	18.09	4.86	.182
$15,000–39,999	18	22.5	31	32.98		
$40,000–69,999	18	22.5	22	23.40		
>$70,000	19	23.75	24	25.53		
Unknown	1	1.25	0	0		

[1]Wave 1 and Wave 2 anxiety were measured by Screen for Child Anxiety-Related Emotional Disorders. Anxiety during COVID-19 (wave 3) was measured by Beck Anxiety Inventory.
[2]Wave 1 and Wave 2 depression were measured by Mood and Feelings Questionnaire. Depression during COVID-19 (Wave 3) was measured using Beck Depression Inventory.
[3]Other/Multiracial group was collapsed with Hispanic/LatinX group for chi-square estimation.
[4]Unknown group was collapsed with <$15,000 group for chi-square estimation.

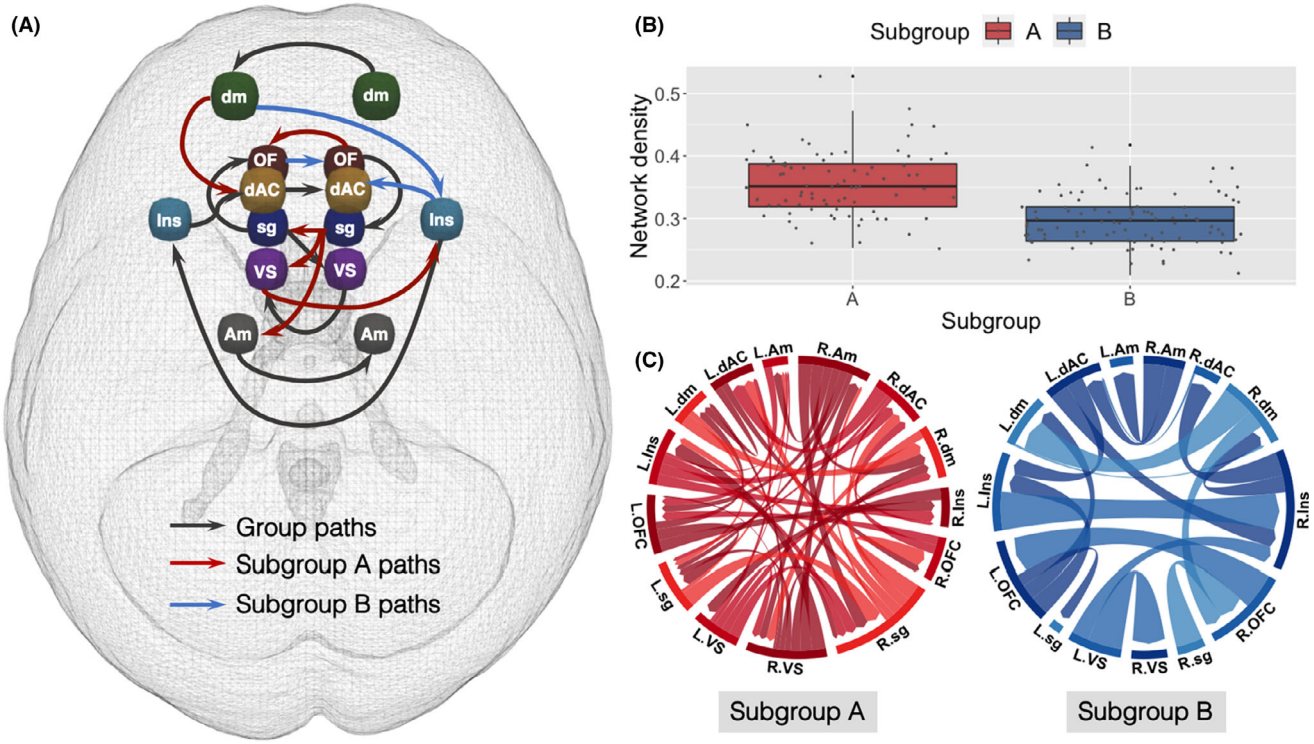

Figure 1 Neural networks derived during an emotion processing task. (A) S-GIMME derived group level, subgroup level, and illustrative individual-level connections. Nodes shown are as follows: amygdala (Am; gray), dorsal anterior cingulate cortex (dAC; yellow), dorsomedial prefrontal cortex (dm; green), insula (Ins; blue), orbitofrontal cortex (OF; dark red), subgenual anterior cingulate cortex (sg; dark blue), and ventral striatum (VS; purple). Eighty ($N = 80$) individuals were clustered into Subgroup A, whereas 94 ($N = 94$) individuals were clustered into Subgroup B. Group-level paths (connections present in at least 75% of the entire sample) are shown in black; subgroup paths (connections present in at least 50% of individuals in each subgroup) are shown in red (Subgroup A) and blue (Subgroup B). Thresholds were default parameters used in connectivity and subgrouping estimation based on large-scale simulations. All connections were positive on average, in exception for left dorsomedial prefrontal cortex (dm) to right insula (Ins) Subgroup B path (all average path estimates reported in Table S8). (B) Network density (i.e., the proportion of actual contemporaneous connections from the number of possible connections in a network) for each individual in Subgroup A (red) and Subgroup B (blue). Network density was significantly greater in Subgroup A compared with Subgroup B ($M_A = .36$, $SD_A = .05$; $M_B = .30$, $SD_B = .04$; $t(147.36) = 8.47$, $p < .001$). (C) Person-specific network maps (i.e., individual-level functional connectivity estimated for each individual in the sample) for one individual in Subgroup A (red) and another individual in Subgroup B (blue). L. and R. indicate left/right hemisphere. Subgroup A individual had a more heterogeneous network, with more connections beyond group- and subgroup-level connections, whereas Subgroup B individual had a more homogenous network, with fewer connections overall but more similar connections to the group- and subgroup-level patterns. All edges shown were contemporaneous, and figures were created using customized R codes and *circlize* package (Gu, Gu, Eils, Schlesner, & Brors, 2014)

Subgroup A network was characterized by greater heterogeneity (i.e., more individual-level connections; $M_A = 17.45$, $SD_A = 4.69$; $M_B = 15$, $SD_B = 3.62$; $t(147.36) = 3.81$, $p < .001$) and relatively greater density compared with subgroup B ($M_A = .36$, $SD_A = .05$; $M_B = .30$, $SD_B = .04$; $t(147.36) = 8.47$, $p < .001$; Figure 1). Moreover, individuals in subgroup A showed significantly greater centrality in the left amygdala ($t(170.72) = 3.93$, $p_{\text{-adjust}} = .002$), right subgenual anterior cingulate ($t(171.19) = 8.92$, $p_{\text{-adjust}} < .001$), and left ventral striatum ($t(167.23) = 8.17$, $p_{\text{-adjust}} < .001$; Figure 2). In contrast, individuals in subgroup B showed significantly greater centrality in the left dorsal anterior cingulate ($t(171.32) = 4.09$, $p_{\text{-adjust}} < .001$) and bilateral insula left: $t(171.14) = 3.28$, $p_{\text{-adjust}} = .017$; right: ($t(167.95) = 4.28$, $p_{\text{-adjust}} < .001$; Figure 2; see Table S5 for comparison of node centrality across subgroups).

Prospective associations of neural network with symptoms

Accounting for initial levels of symptoms, subgroup A membership predicted greater change in anxiety over time ($\beta = .138$, $p = .042$) relative to subgroup B, and these subgroup differences remained after adjusting for main covariates ($\beta = .194$, $p = .023$; Table 2) and additional covariates ($\beta = .257$, $p = .011$; Table S6). Results were specific to anxiety: subgroup membership did not predict change in depression ($\beta = .089$, $p = .243$; Table 2; Figure 3). When examining specific ROIs, individual node centrality did not predict a change in anxiety or depression after Bonferroni correction for multiple comparisons (Table S7). Sex differences in symptoms were most pronounced at age 15 when both anxiety ($\beta = .342$, $p < .001$) and depressive ($\beta = .348$, $p < .001$) symptoms were more prevalent in females

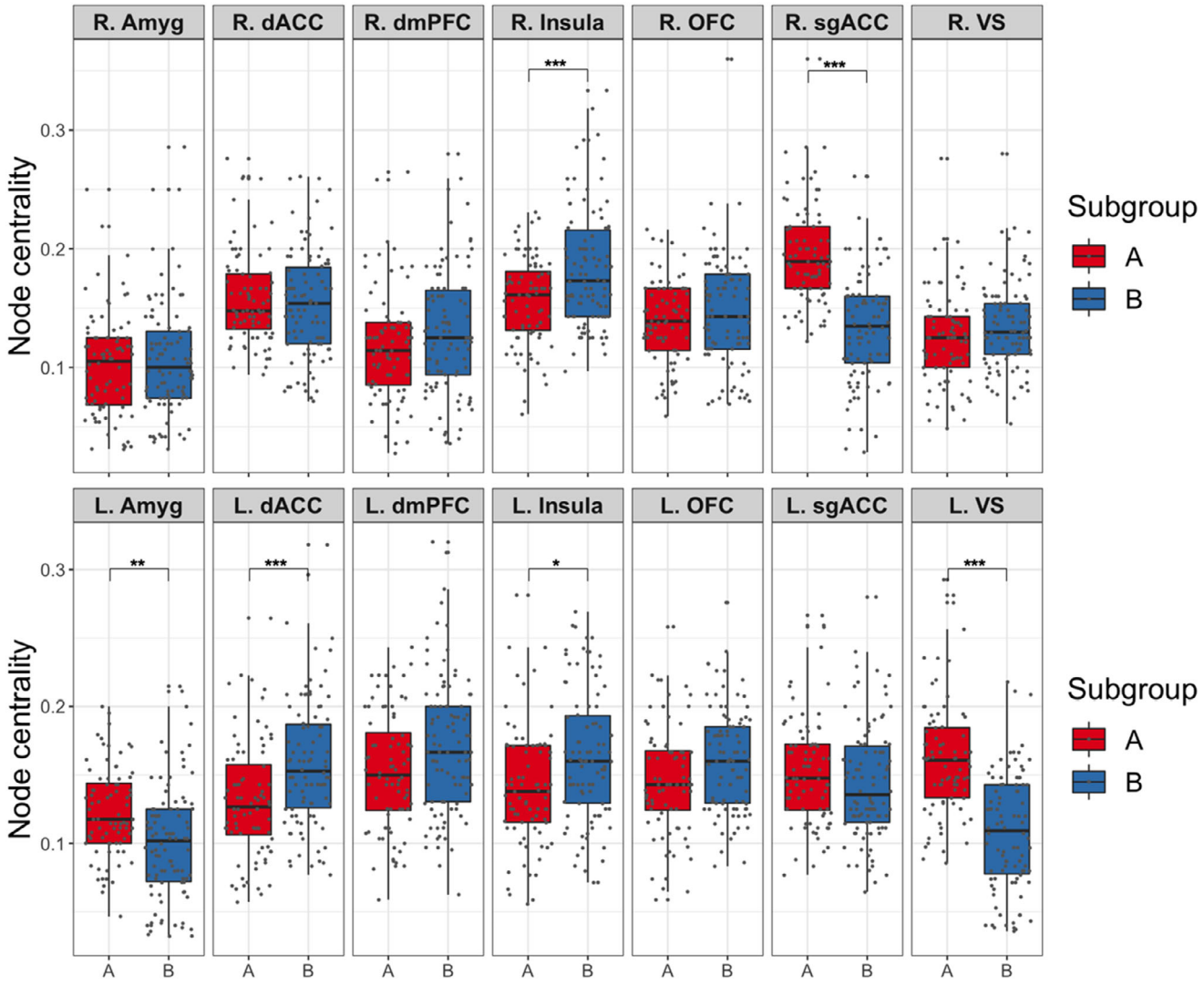

Figure 2 Node centrality across each ROI plotted for each subgroup. ***Bonferroni-corrected $p < .001$, **Bonferroni-corrected $p < .01$, *Bonferroni-corrected $p < .05$. Left to right: amygdala (Amyg), dorsal anterior cingulate (dACC), dorsomedial prefrontal cortex (dmPFC), insula, orbitofrontal (OFC), subgenual anterior cingulate (sgACC), ventral striatum (VS). Hemispheres denoted by R. and L. Compared with Subgroup B (blue), Subgroup A (red) shows significantly greater node centrality, specifically in the left amygdala (L.Amyg), left striatum (L.VS), and right subgenual anterior cingulate (R.sgACC). In contrast, Subgroup B shows greater node centrality in the left dorsal anterior cingulate (L.dACC) and bilateral insula (R.Insula, L.Insula). *p* Values were Bonferroni-corrected for multiple comparisons (Table S5)

than males (Figure S5), but symptoms did not differ across sex during the pandemic (anxiety: $\beta = .075$, $p = .420$; depression: $\beta = .020$, $p = .829$). Additionally, there were no subgroup–sex interactions predicting anxiety ($\beta = -.0005$, $p = .997$) or depression ($\beta = .070$, $p = .644$) during the pandemic. These results pertained to a functional network of hypothesized ROIs; there were no subgroup differences in symptoms from prediction analyses using the comparison network (i.e., a nonhypothesized set of ROIs; see Appendix S5 and Table S4).

Susceptibility to COVID-19 economic adversity

Increased economic adversity during the pandemic was related to greater anxiety symptoms during COVID-19 across all participants ($\beta = .367$, $p < .001$). Moreover, there was a significant adversity–subgroup interaction ($\beta = .307$, $p = .006$), such that participants in the more heterogeneous Subgroup A reported greater anxiety during the pandemic in response to pandemic-related economic adversity relative to subgroup B (Figure 4), and this interaction effect remained after adjusting for the initial level of anxiety and covariates ($\beta = .237$, $p = .021$; Table 3), and additional covariates ($\beta = .259$, $p = .031$; Table S6). There was a similar association in which economic adversity was associated with depression across all participants ($\beta = .356$, $p < .001$), but adversity–subgroup interaction effect was not statistically significant for depression ($\beta = .196$, $p = .088$; Figure 4). Subgroups did not statistically differ in their reports of COVID-19 economic adversity (Table 1). Furthermore, subgroup–adversity interaction did not predict symptoms when analyses were done using subgroups that were derived from the comparison network (i.e., a nonhypothesized set of ROIs; see Appendix S5; Table S4).

Table 2 Results from models predicting change in anxiety and depressive symptoms over time using subgroups while adjusting for initial symptoms (model 1) and covariates (model 2)

	Change in anxiety				Change in depression			
	Model 1		Model 2		Model 1		Model 2	
	β	*p*	β	*p*	β	*p*	β	*p*
Subgroup (A)	.138	.042	.194	.023	.089	.243	.120	.194
Initial symptoms	−.456	<.001	−.379	<.001	−.100	0.189	.072	.432
Male			.068	.538			.210	.080
Puberty			.008	.937			−.030	.798
Age			.086	.308			.018	.846
White			.160	.078			−.060	.539
Hispanic			−.011	.898			.098	.281
Other			−.118	.155			−.103	.252
Baseline income			.031	.726			.089	.351
Pandemic duration			.022	.795			−.093	.310
	$F(2,170) = 24.56$, $p < .001$		$F(10,120) = 3.82$, $p < .001$		$F(2,170) = 1.46$, $p = .235$		$F(10,120) = 1.31$, $p = .233$	

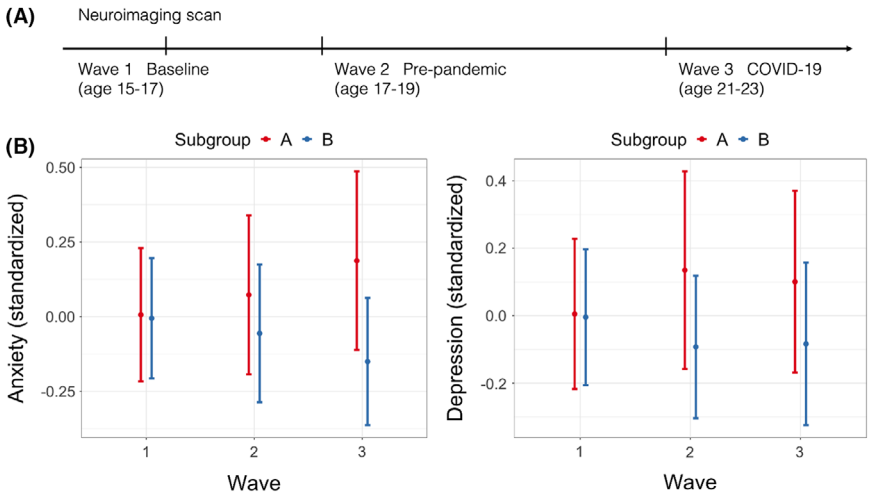

Figure 3 Anxiety and depressive symptoms across three waves. (A) Illustration of timepoints and ages at each wave of data collection. (B) Anxiety and depression for each subgroup (A: more heterogeneous network with greater centrality in the amygdala, subgenual, and striatum and B: relatively sparser network with greater centrality in the insula and dorsal anterior cingulate) across each wave. Participants across subgroups did not differ in initial anxiety and depression at wave 1, but symptoms began to diverge at wave 2, which persisted through wave 3. For anxiety, this divergence was exacerbated by COVID-19 at wave 3, whereas subgroup difference for depression during COVID-19 remained similar to prepandemic difference. Each point represents mean values, and the bars indicate standard errors

Discussion

Using a person-specific functional neural connectivity mapping, data-driven subgroups prospectively predicted increasing anxiety and stress susceptibility during a highly stressful event. Two subgroups emerged, a more heterogeneous subgroup characterized by relatively greater variation in person-specific networks and greater network density as well as more connections involving the amygdala, subgenual anterior cingulate, and striatum and a more homogenous subgroup, characterized by lower network density and greater involvement of the insula and dorsal anterior cingulate cortex. Relative to individuals in the more homogenous subgroup, individuals in the more heterogeneous subgroup experienced escalating trajectories of anxiety symptoms from age 15 to 21 (during COVID-19 pandemic) when adjusting for initial symptoms. Moreover, despite exposure to equivalent amounts of economic adversity during the pandemic, the more heterogeneous subgroup experienced greater anxiety as economic adversity increased, and the results remained after controlling for initial levels of anxiety at adolescence and other covariates. These results identify potential neural signatures of susceptibility and resiliency to anxiety-related stress. These conclusions are strengthened by the use of an unsupervised data-driven and personalized approach to network mapping using a 6-year longitudinal population-based sample with a substantial representation of marginalized participants who are at greater risk for adversity exposure.

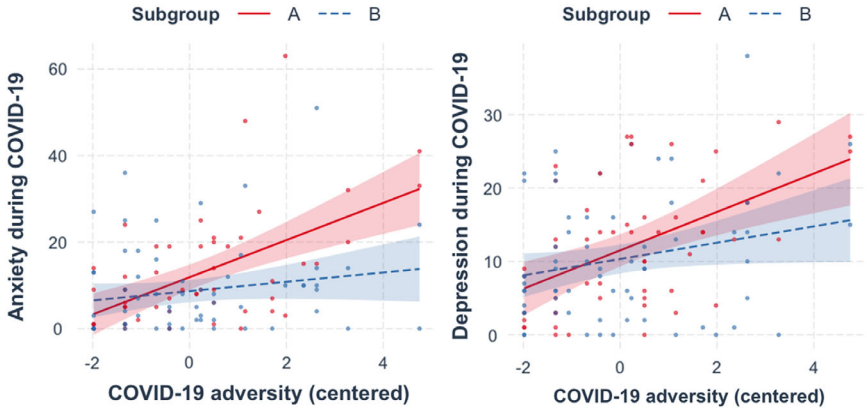

Figure 4 Differential effects of COVID-19 economic adversity on anxiety and depression across neural-based subgroups. Symptoms during COVID-19 (wave 3) were elevated as a function of COVID-19 economic adversity, especially for subgroup A. Subgroup–adversity interaction was significant for anxiety (b = .275, 95% CI = [.470, .080], p = .006), but not depression (b = .175, 95% CI = [−.026, .376], p = .088). Subgroup A slope is depicted in red and Subgroup B slope in blue. COVID-19 adversity scores were mean-centered to aid interpretation. LEFT: Subgroup–adversity interaction for anxiety symptoms. Subgroup A slope (b = .366, 95% CI = [.218, .514], p < .001); Subgroup B slope (b = .092, 95% CI = [−.035, .219], p = .154). RIGHT: Subgroup–adversity interaction for depressive symptoms. Subgroup A slope (b = .304, 95% CI = [.151, .457], p < .001); Subgroup B slope (b = .129, 95% CI = [−.001, .260], p = .053)

Table 3 Results examining subgroup differences in the associations between COVID-19 economic adversity and anxiety/depressive symptoms during the pandemic

	Anxiety during pandemic				Depression during pandemic			
	Model 1		Model 2		Model 1		Model 2	
	β	*p*	β	*p*	β	*p*	β	*p*
Subgroup (A)	.136	.106	.181	.024	.069	.428	.048	.473
COVID-19 adversity	.157	.154	.177	.105	.223	.053	.141	.127
Subgroup (A) × adversity	.307	.006	.237	.021	.196	.088	.069	.420
Initial symptoms			.399	<.001			.710	<.001
Gender			.016	.877			.068	.416
Puberty			.055	.574			−.023	.778
Age			.095	.237			.005	.935
White			.207	.015			−.009	.901
Hispanic			.036	.641			.136	.037
Other			−.048	.537			−.001	.989
Baseline income			.067	.435			.056	.434
Pandemic duration			−.008	.924			−.073	.272
	$F(3,114) = 10.23$, $p < .001$		$F(12,104) = 6.76$, $p < .001$		$F(3,114) = 6.97$, $p < .001$		$F(12,104) = 13.18$, $p < .001$	

The distinction across subgroups in the progression of anxiety symptoms and in relation to adversity demonstrates how network analysis was able to identify individuals whose anxiety symptoms would generally worsen across adolescence and particularly, in response to increased adversity. Notably, reported economic adversity during the pandemic was comparable across the neural subgroups, suggesting that this finding was not driven by disparity in experienced stress, but by individual differences in stress response. Furthermore, though rates of anxiety and depression are often higher in women (Kessler et al., 1994), we found that this sex difference was diminished during the pandemic, and there was no evidence that sex interacted with subgroup membership, nor was a confounder in findings. Thus, these networks appear to be relevant for both men and women. These results are broadly consistent with the biological sensitivity to context model (Boyce & Ellis, 2005), which posits that some individuals are more susceptible to the environment (in this case, economic adversity). However, here we only tested susceptibility related to a negative outcome, leaving open the question of whether these individuals would also achieve more favorable outcomes in a more positive environment.

These results also suggest that more heterogeneous adolescent neural networks, specifically those involving the amygdala, subgenual cingulate, and striatum, may indicate sensitivity to future stress. Individuals with greater heterogeneity in their networks (i.e., more connections that were different from connectivity patterns found in all participants) and greater network density (i.e., more connections among ROIs) showed greater increases in anxiety and susceptibility to stress. These results are consistent with evidence showing

that greater reactivity of emotion-related regions predicts risk for psychopathology (Greicius et al., 2007; Schwartz, Wright, Shin, Kagan, & Rauch, 2003; Stein, Simmons, Feinstein, & Paulus, 2007). Furthermore, greater heterogeneity in the more susceptible group in the present investigation suggests that psychopathology may be related to more variations in neural connectivity, consistent with the notion that there may be a greater neural heterogeneity in biological features of psychopathology and fewer variations in neural patterns (i.e., homogeneity) in the general population (Fair, Bathula, Nikolas, & Nigg, 2012; Feczko et al., 2019; Finn et al., 2020). Notably, the detection of neural heterogeneity in the present study was accomplished by clustering individuals using their personalized neural networks, thus demonstrating the strength of person-specific connectivity mapping in teasing apart similarities and differences in neural patterns the prediction of mental health phenotypes. These inferences can be strengthened by future investigations that examine whether such heterogeneity persists with time, or whether neural function converges to more homogenous patterns of connectivity with improvements in symptomatology. Furthermore, future research can benefit from further testing of whether there are other neural networks implicated in stress susceptibility beyond the brain regions examined in the present investigation.

The present results identified distinct responses to stress within an important sample of participants who represent identities and groups that are underrepresented in biomedical research during a historic global event. Though one neural network-based subgroup did appear to be more susceptible to pandemic-related adversity, the other group was relatively resilient, at least on the measures we examined. Evidence of this type of resilience is critical in identifying why and how some individuals thrive despite adversity, particularly for those facing increased stress via marginalization and oppression. Even with compounding economic stress, health-related distress, police brutality, and other forms of social unrest that occurred during the pandemic, individuals with sparser adolescent functional networks and more connections involving the insula and dorsal anterior cingulate showed remarkable resilience against accumulating stressors. These findings echo clinical studies showing increased connectivity between the insula and dorsal anterior cingulate in nonanxious individuals (Klumpp, Angstadt, & Phan, 2012), which suggests that adaptive mechanisms involving these regions may be protective against stress. More research is thus needed to identify mechanisms through which resilience can be bolstered for individuals that are facing chronically high stress.

Results showing significant effects for anxiety but not depression are consistent with recent findings on the mental health impact of the COVID-19 pandemic (He et al., 2021; Zeytinoglu et al., 2021). There may be several explanations for these findings. First, the pandemic and economic adversity may have a more immediate effect on anxiety in the short-term, compared with depression, which may require a longer time to manifest. Unpredictable external situations such as the pandemic may provoke cognitive states of heightened threat that is more aligned with anxious schemas (Beck & Clark, 1988), and since our measures of symptoms were taken within the first year of the pandemic, we may have captured the rise in anxiety before a later rise in depression (that occurred as the stress became more chronic). Second, our results demonstrate that the group difference in the associations between economic adversity and symptoms was more pronounced for anxiety, suggesting that both groups may be equally more depressed as a function of the economic impact of the pandemic. Third, these findings may indicate potential distinct circuitries between anxiety and depression (Wang et al., 2021), but given that our study had only tested for networks within selected regions, more research is needed to test the specific processes that are driving these differences.

Though our study is buoyed by several strengths, including prospective longitudinal data of underrepresented individuals and the use of computational methods, there are several limitations. First, COVID-19 adversity was measured at the same time as anxiety and depression; thus, determination of the direction of links between adversity and symptoms is not possible. Nevertheless, the positive associations between adversity and symptoms suggest an increase in psychological distress that was accompanied by increased adversity. Second, we were not able to collect data from all participants from FFCWS that we attempted to recruit, nor did all participants in the neuroimaging study participate at all three waves reported here; however, sampling attrition is expected in longitudinal studies, and included sample did not differ demographically across included waves. Third, anxiety and depression were measured using the same scale at wave 1 and wave 2, but not wave 3 because the measures were shifted to be more developmentally appropriate, changing from well-validated adolescent to adult measures at age 20 (Wang & Gorenstein, 2013). Nonetheless, correlations between these measures were comparable, suggesting measurement correspondence across waves. Fourth, as with many other neuroimaging studies, the present analyses were conducted with the assumption of functional-structural correspondence across participants. The use of the same location for ROIs across individuals facilitates the estimation of similarities between people and the detection of subgroup membership. Finally, we recognize the limitations of our modestly sized sample; however, this study examined within-person symptomatic change that provides critical information about underrepresented individuals during a notable historical period; within-person analyses can boost power and reliability (Curran & Bauer, 2011). Furthermore, the reliability of the data

and methods we utilized for subgrouping and functional connectivity estimation was demonstrated by additional checks (i.e., split-half, 80% test), which reflected the robustness of model estimation across split-half of the functional data and subsets of the sample (see Appendix S9).

Conclusion

In this 6-year prospective study, a data-driven adolescent neural network characterized by relatively more heterogeneity and density involving the amygdala, subgenual cingulate, and striatal regions identified a subgroup of individuals with increasing anxiety symptoms that further increased during COVID-19. These findings demonstrate potential neural features indicating susceptibility to future stress, which may confer risk and resilience for mental health in young adults who are making the important transition to adulthood.

Supporting information

Additional supporting information may be found online in the Supporting Information section at the end of the article:

Appendix S1. Exclusions for neuroimaging scan.
Appendix S2. MRI data acquisition and preprocessing.
Appendix S3. fMRI task paradigm.
Appendix S4. ROI selection and data extraction.
Appendix S5. Comparison network.
Appendix S6. Measures for anxiety and depressive symptoms.
Appendix S7. Covariates.
Appendix S8. S-GIMME.
Appendix S9. Robustness checks for functional connectivity estimation.
Appendix S10. Robustness checks in predictive models.
Figure S1. Exclusionary criteria for neuroimaging data.
Figure S2. fMRI task paradigm.
Figure S3. S-GIMME flowchart.
Figure S4. GIMME results based on five randomly drawn 80% subsamples.
Figure S5. Anxiety and depression for each subgroup, stratified by sex.
Table S1. Full and included sample comparisons[a].
Table S2. MNI coordinates of individual Regions of Interest (ROI).
Table S3. MNI coordinates of ROIs in comparison network.
Table S4. Results from predictive models using comparison network.
Table S5. Node centrality for each subgroup.
Table S6. Results from predictive models predicting anxiety and depressive symptoms including all covariates.
Table S7. Individual node centrality predicting change in symptoms, adjusting for initial levels (tested in separate models).
Table S8. Average path estimates for group- and subgroup-level connections.
Table S9. Comparison between extracted data using 4mm-radii node spheres and 6.5mm-radii node spheres.
Table S10. Results from split-half reliability test ($N = 174$).
Table S11. Results from 80% randomly drawn subsample test.

Acknowledgements

This work was supported by funds from the National Institute of Health: R01MH103761 (PI: C.S.M.), R01MH121079 (PIs: C.S.M., C.M., L.W.H.), 3R01MH121079-02S1 (PIs: C.S.M., C.M., L.W.H.), T32HD007109 (PIs: C.S.M., V.M.), 1S10OD012240 (PI: Noll). Study participants provided informed consent or assent (when minors, with parent consent) at all timepoints. Study protocols were approved by the University of Michigan ethics committee (IRB: HUM00167754; HUM00074392). The authors have declared that they have no competing or potential conflict of interest.

Correspondence

Christopher S. Monk, Department of Psychology, University of Michigan, 2030 East Hall, 530 Church St, Ann Arbor, MI 48109-1043, USA;
Email: csmonk@umich.edu

Key points

- Longitudinal study spanning 6 years examined adolescent data-driven functional networks to prospectively predict adult anxiety and susceptibility to future stress.
- Those with networks that were more heterogeneous (i.e., greater person-specific variations) with more connections involving the amygdala, subgenual cingulate, and striatum were more susceptible to economic adversity during COVID-19, compared to those with more homogenous networks involving insula and dorsal anterior cingulate.
- Findings can inform intervention and prevention efforts by identifying neural profiles of individuals who are susceptible to stress related to anxiety.

References

Bassett, D.S., & Bullmore, E.T. (2017). Small-world brain networks revisited. *The Neuroscientist*, *23*, 499–516.

Beck, A.T., & Clark, D.A. (1988). Anxiety and depression: An information processing perspective. *Anxiety Research*, *1*, 23–36.

Beltz, A., Dotterer, H., & Goetschius, L. (2019). GIMME preprocessing: Initial release (version v1. 0). *Zenodo*. doi: 10.5281/zenodo.2692522

Beltz, A.M., & Gates, K.M. (2017). Network mapping with GIMME. *Multivariate Behavioral Research*, *52*, 789–804.

Boyce, W.T., & Ellis, B.J. (2005). Biological sensitivity to context: I. An evolutionary–developmental theory of the origins and functions of stress reactivity. *Development and Psychopathology*, *17*, 271–301.

Bullmore, E., & Sporns, O. (2009). Complex brain networks: Graph theoretical analysis of structural and functional systems. *Nature Reviews Neuroscience*, *10*, 186–198.

Curran, P.J., & Bauer, D.J. (2011). The disaggregation of within-person and between-person effects in longitudinal models of change. *Annual Review of Psychology*, *62*, 583–619.

Elliott, M.L., Knodt, A.R., Ireland, D., Morris, M.L., Poulton, R., Ramrakha, S., … & Hariri, A.R. (2020). What is the test-retest reliability of common task-functional MRI measures? New empirical evidence and a meta-analysis. *Psychological Science*, *31*, 792–806.

Etkin, A., & Wager, T.D. (2007). Functional neuroimaging of anxiety: A meta-analysis of emotional processing in PTSD, social anxiety disorder, and specific phobia. *American Journal of Psychiatry*, *164*, 1476–1488.

Fair, D.A., Bathula, D., Nikolas, M.A., & Nigg, J.T. (2012). Distinct neuropsychological subgroups in typically developing youth inform heterogeneity in children with ADHD. *Proceedings of the National Academy of Sciences of the United States of America*, *109*, 6769–6774.

Falk, E.B., Hyde, L.W., Mitchell, C., Faul, J., Gonzalez, R., Heitzeg, M.M., … & Schulenberg, J. (2013). What is a representative brain? Neuroscience meets population science. *Proceedings of the National Academy of Sciences of the United States of America*, *110*, 17615–17622.

Feczko, E., Miranda-Dominguez, O., Marr, M., Graham, A.M., Nigg, J.T., & Fair, D.A. (2019). The heterogeneity problem: Approaches to identify psychiatric subtypes. *Trends in Cognitive Sciences*, *23*, 584–601.

Finn, E.S. (2021). Is it time to put rest to rest? *Trends in Cognitive Sciences*, *25*, 1021–1032.

Finn, E.S., Glerean, E., Khojandi, A.Y., Nielson, D., Molfese, P.J., Handwerker, D.A., & Bandettini, P.A. (2020). Idiosynchrony: From shared responses to individual differences during naturalistic neuroimaging. *NeuroImage*, *215*, 116828.

Finn, E.S., Scheinost, D., Finn, D.M., Shen, X., Papademetris, X., & Constable, R.T. (2017). Can brain state be manipulated to emphasize individual differences in functional connectivity? *NeuroImage*, *160*, 140–151.

Gates, K.M., Lane, S.T., Varangis, E., Giovanello, K., & Guiskewicz, K. (2017). Unsupervised classification during time-series model building. *Multivariate Behavioral Research*, *52*, 129–148.

Gates, K.M., & Molenaar, P.C.M. (2012). Group search algorithm recovers effective connectivity maps for individuals in homogeneous and heterogeneous samples. *NeuroImage*, *63*, 310–319.

Goetschius, L.G., Hein, T.C., McLanahan, S.S., Brooks-Gunn, J., McLoyd, V.C., Dotterer, H.L., … & Beltz, A.M. (2020). Association of childhood violence exposure with adolescent neural network density. *JAMA Network Open*, *3*, e2017850.

Gordon, E.M., Laumann, T.O., Gilmore, A.W., Newbold, D.J., Greene, D.J., Berg, J.J., … & Dosenbach, N.U.F. (2017). Precision functional mapping of individual human brains. *Neuron*, *95*, 791–807.e7.

Greene, A.S., Gao, S., Scheinost, D., & Constable, R.T. (2018). Task-induced brain state manipulation improves prediction of individual traits. *Nature Communications*, *9*, 2807.

Greicius, M.D., Flores, B.H., Menon, V., Glover, G.H., Solvason, H.B., Kenna, H., … & Schatzberg, A.F. (2007). Resting-state functional connectivity in major depression: Abnormally increased contributions from subgenual cingulate cortex and thalamus. *Biological Psychiatry*, *62*, 429–437.

Gu, Z., Gu, L., Eils, R., Schlesner, M., & Brors, B. (2014). Circlize implements and enhances circular visualization in R. *Bioinformatics*, *30*, 2811–2812.

He, L., Wei, D., Yang, F., Zhang, J., Cheng, W., Feng, J., … & Qiu, J. (2021). Functional connectome prediction of anxiety related to the COVID-19 pandemic. *American Journal of Psychiatry*, *178*, 530–540.

Hein, T.C., Goetschius, L.G., McLoyd, V.C., Brooks-Gunn, J., McLanahan, S.S., Mitchell, C., … & Monk, C.S. (2020). Childhood violence exposure and social deprivation are linked to adolescent threat and reward neural function. *Social Cognitive and Affective Neuroscience*, *15*, 1252–1259.

Janiri, D., Moser, D.A., Doucet, G.E., Luber, M.J., Rasgon, A., Lee, W.H., … & Frangou, S. (2020). Shared neural phenotypes for mood and anxiety disorders: A meta-analysis of 226 task-related functional imaging studies. *JAMA Psychiatry*, *77*, 172–179.

Kessler, R.C., Berglund, P., Demler, O., Jin, R., Merikangas, K.R., & Walters, E.E. (2005). Lifetime prevalence and age-of-onset distributions of DSM-IV disorders in the national comorbidity survey replication. *Archives of General Psychiatry*, *62*, 593–602.

Kessler, R.C., McGonagle, K.A., Zhao, S., Nelson, C.B., Hughes, M., Eshleman, S., … & Kendler, K.S. (1994). Lifetime and 12-month prevalence of DSM-III-R psychiatric disorders in the United States: Results from the National Comorbidity Survey. *Archives of General Psychiatry*, *51*, 8–19.

Klumpp, H., Angstadt, M., & Phan, K.L. (2012). Insula reactivity and connectivity to anterior cingulate cortex when processing threat in generalized social anxiety disorder. *Biological Psychology*, *89*, 273–276.

Kragel, P.A., Han, X., Kraynak, T.E., Gianaros, P.J., & Wager, T.D. (2021). Functional MRI can be highly reliable, but it depends on what you measure: A commentary on Elliott et al. (2020). *Psychological Science*, *32*, 622–626.

Lane, S.T., Gates, K.M., Pike, H.K., Beltz, A.M., & Wright, A.G.C. (2019). Uncovering general, shared, and unique temporal patterns in ambulatory assessment data. *Psychological Methods*, *24*, 54–69.

Lütkepohl, H. (2005). *New introduction to multiple time series analysis*. Berlin, DE: Springer Science & Business Media.

Mattson, W.I., Hyde, L.W., Shaw, D.S., Forbes, E.E., & Monk, C.S. (2016). Clinical neuroprediction: Amygdala reactivity predicts depressive symptoms 2 years later. *Social Cognitive and Affective Neuroscience*, *11*, 892–898.

McLaughlin, K.A., & Nolen-Hoeksema, S. (2012). Interpersonal stress generation as a mechanism linking rumination to internalizing symptoms in early adolescents. *Journal of Clinical Child & Adolescent Psychology*, *41*, 584–597.

Noble, S., Scheinost, D., & Constable, R.T. (2021). A guide to the measurement and interpretation of fMRI test-retest reliability. *Current Opinion in Behavioral Sciences*, *40*, 27–32.

Price, J.L., & Drevets, W.C. (2010). Neurocircuitry of mood disorders. *Neuropsychopharmacology*, *35*, 192–216.

Reichman, N.E., Teitler, J.O., Garfinkel, I., & McLanahan, S.S. (2001). Fragile families: Sample and design. *Children and Youth Services Review*, *23*, 303–326.

Robinson, C., & Schumacker, R.E. (2009). Interaction effects: Centering, variance inflation factor and interpretation issues. *Multiple Linear Regression Viewpoints*, *35*, 6–11.

Schwartz, C.E., Wright, C.I., Shin, L.M., Kagan, J., & Rauch, S.L. (2003). Inhibited and uninhibited infants "grown up": Adult Amygdalar response to novelty. *Science*, *300*, 1952–1953.

Stein, M.B., Simmons, A.N., Feinstein, J.S., & Paulus, M.P. (2007). Increased amygdala and insula activation during emotion processing in anxiety-prone subjects. *American Journal of Psychiatry*, *164*, 318–327.

Swartz, J.R., Knodt, A.R., Radtke, S.R., & Hariri, A.R. (2015). A neural biomarker of psychological vulnerability to future life stress. *Neuron*, *85*, 505–511.

Tai, D.B.G., Shah, A., Doubeni, C.A., Sia, I.G., & Wieland, M.L. (2021). The disproportionate impact of COVID-19 on racial and ethnic minorities in the United States. *Clinical Infectious Diseases*, *72*, 703–706.

Taxali, A., Angstadt, M., Rutherford, S., & Sripada, C. (2021). Boost in test–retest reliability in resting state fMRI with predictive modeling. *Cerebral Cortex*, *31*, 2822–2833.

Wang, Y.-P., & Gorenstein, C. (2013). Psychometric properties of the Beck Depression Inventory-II: A comprehensive review. *Revista Brasileira de Psiquiatria*, *35*, 416–431.

Wang, Z., Goerlich, K.S., Ai, H., Aleman, A., Luo, Y., & Xu, P. (2021). Connectome-based predictive modeling of individual anxiety. *Cerebral Cortex*, *31*, 3006–3020.

Woodcock, R.W., McGrew, K.S., & Mather, N. (2001). *Woodcock-Johnson III NU Complete*. Rolling Meadows, IL: Riverside Publishing.

Xiong, J., Lipsitz, O., Nasri, F., Lui, L.M.W., Gill, H., Phan, L., … & McIntyre, R.S. (2020). Impact of COVID-19 pandemic on mental health in the general population: A systematic review. *Journal of Affective Disorders*, *277*, 55–64.

Yarkoni, T., Poldrack, R.A., Nichols, T.E., Van Essen, D.C., & Wager, T.D. (2011). Large-scale automated synthesis of human functional neuroimaging data. *Nature Methods*, *8*, 665–670.

Zeytinoglu, S., Morales, S., Lorenzo, N.E., Chronis-Tuscano, A., Degnan, K.A., Almas, A.N., … & Fox, N.A. (2021). A developmental pathway from early behavioral inhibition to young Adults' anxiety during the COVID-19 pandemic. *Journal of the American Academy of Child & Adolescent Psychiatry*, *60*, 1300–1308.

Accepted for publication: 10 November 2022